THE JOURNAL OF PHYSICAL CHEMISTRY C

Article

pubs.acs.org/JPCC

Electron-Induced Chemistry of Cobalt Tricarbonyl Nitrosyl ($Co(CO)_3NO$) in Liquid Helium Nanodroplets

Johannes Postler,[†] Michael Renzler,[†] Alexander Kaiser,[†] Stefan E. Huber,[†] Michael Probst,[†] Paul Scheier,*[,†] and Andrew M. Ellis*[,‡]

[†]Institut für Ionenphysik und Angewandte Physik, Universität Innsbruck, Technikerstr. 25, A-6020 Innsbruck, Austria

[‡]Department of Chemistry, University of Leicester, University Road, Leicester, LE1 7RH, U. K.

ABSTRACT: Electron addition to cobalt tricarbonyl nitrosyl ($Co(CO_3NO$) and its clusters has been explored in helium nanodroplets. Anions were formed by adding electrons with controlled energies, and reaction products were identified by mass spectrometry. Dissociative electron attachment (DEA) to the $Co(CO)_3NO$ monomer gave reaction products similar to those reported in earlier gas phase experiments. However, loss of NO was more prevalent than loss of CO, in marked contrast to the gas phase. Since the Co−N bond is significantly stronger than the Co−C bond, this preference for NO loss must be driven by selective reaction dynamics at low temperature. For $[Co(CO)_3NO]_N$ clusters, the DEA chemistry is similar to that of the monomer, but the anion yields as a function of electron energy show large differences, with the relatively sharp resonances of the monomer being replaced by broad profiles peaking at much higher electron energies. A third experiment involved DEA of $Co(CO)_3NO$ on a C_{60} molecule in an attempt to simulate the effect of a surface. Once again, broad ion yield curves are seen, but CO loss now becomes the most probable reaction channel. The implication of these findings for understanding focused electron beam induced deposition of cobalt is described.

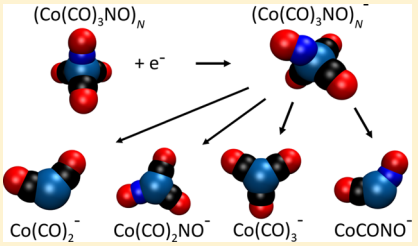

INTRODUCTION

Focused electron beam induced deposition (FEBID), which also goes by the alternative names of focused electron beam induced processing (FEBIP) or simply as electron beam induced deposition (EBID), is a promising technique for the direct "writing" of patterns onto solid surfaces.[1−3] It operates at a resolution approaching 1 nm and can be regarded as a variant of chemical vapor deposition in which a focused beam of electrons induces decomposition in a volatile precursor, leading to deposition of the desired material. The deposition of metals is commonly achieved in FEBID using volatile-metal-containing complexes, which, in addition to their high vapor pressures, are often relatively easy to decompose because of low binding energies between the metal atom and the surrounding ligands.

While FEBID shows great promise, it also has limitations. One problem is the incorporation of nonmetallic impurities into metal deposits, which can arise for several reasons, including incomplete dissociation of the precursor, recombination reactions on the substrate surface, or the electron-induced production of involatile nonmetallic species such as carbon clusters. Another well-known problem is broadening of the deposited structures relative to the diameter of the focused electron beam, a process which is often ascribed to dissociative electron attachment (DEA). DEA can give rise to a loss of pattern resolution because low energy secondary electrons and electrons that are inelastically backscattered from the substrate can attach to precursor molecules outside of the primary excitation zone and then initiate decomposition chemistry.

As a result of these limitations and to try and find ways of mitigating them, it is important to understand the DEA mechanisms for common FEBID precursor molecules. One such molecule is cobalt tricarbonyl nitrosyl, $Co(CO)_3NO$, which has recently been used as an alternative to $Co_2(CO)_8$ to deposit cobalt using FEBID.[4−6] The deposition of cobalt nanostructures is particularly interesting because of the ferromagnetic properties of this element, which might be exploited in devices such as nanoscale Hall sensors[7,8] and magnetic force microscopy tips.[9] The DEA mechanism for gaseous $Co(CO)_3NO$ has recently been explored for the first time by Engmann et al.[10−12] Absolute DEA cross sections were established in this work, and mechanistic information was extracted, including evidence that the first step involves predominantly CO loss. Another recent study has investigated the electron-induced decomposition of a nanofilm of $Co(CO)_3NO$ on a solid substrate and employed surface science techniques, such as X-ray photoelectron spectroscopy, to extract mechanistic information.[13] As in the gas phase, decomposition on a surface seems to involve facile loss of CO. However, in the surface study, there was clear evidence of formation of a nitride as the initial step, i.e.

$$Co(CO)_3NO\ (adsorbed) + e^- \rightarrow CoN(CO)_mO\ (adsorbed) + other\ products + e^- \quad (1)$$

Received: June 3, 2015
Revised: August 11, 2015
Published: August 11, 2015

DOI: 10.1021/acs.jpcc.5b05260
J. Phys. Chem. C 2015, 119, 20917−20922

The formation of a relatively stable CoN entity is consistent with the observation that the level of nitrogen in FEBID deposits derived from $Co(CO)_3NO$ is usually greater than carbon.[4,5] It should be noted that the surface study by Rosenberg et al.[13] used electrons with 500 eV kinetic energy, which is much higher than the electron energies used in the gas phase work by Engmann et al.[10,11]

Here, we adopt a different approach for exploring the DEA mechanism of $Co(CO)_3NO$. This involves isolating the precursor in a liquid helium nanodroplet, where electrons of defined energy are then subsequently added to induce chemistry. One of the advantages of working with helium droplets is the possibility of using the liquid helium to rapidly quench reactions, thus making it more likely to detect intermediate reaction products. Such information has the potential to generate new insight into the DEA mechanism. In addition, by increasing the doping rate, it is straightforward to add multiple precursor molecules to a helium nanodroplet, which makes it possible to see if the DEA mechanism is altered by clustering. Information of this type is potentially highly significant, since, in FEBID, the decomposition is likely to take place on a substrate surface and within a thin precursor film, rather than via individual isolated molecules in the gas phase.[13−15] Thus, the current study can potentially bridge the gap between a purely gas phase study of the DEA mechanism of the $Co(CO)_3NO$ monomer and a study of the decomposition of a thin $Co(CO)_3NO$ film.

A third advantage of working with helium nanodroplets, which we also exploit here, is that it is possible to add another species to the droplets to act as a model substrate on which to initiate chemistry. In this study, we choose C_{60} as the substrate.

We find that the electron-induced decomposition of a single $Co(CO)_3NO$ complex in a helium droplet has much in common with the same molecule in the gas phase. However, as will be discussed, the reaction probabilities are not identical. Furthermore, the anion yields as a function of electron energy change dramatically when switching either to $[Co(CO)_3NO]_N$ clusters or to a single complex located on a C_{60} surface. This suggests that, while DEA studies of the monomer are a valuable starting point, the DEA behavior of FEBID precursor molecules on a solid surface will differ substantially from the gas phase scenario.

EXPERIMENTAL SECTION

Full details of the experimental setup and the general operating procedure can be found elsewhere.[16] Briefly, helium nanodroplets were produced by expanding high purity gaseous helium at a stagnation pressure of 21 bar and a temperature of 9.4 K through a 5 μm pinhole into a vacuum. Under these conditions, the average number of helium atoms per droplet was in the region of 4×10^5.[17] The expansion was skimmed to form a collimated droplet beam, and this was then passed through a pick-up cell containing vapor of $Co(CO)_3NO$ (Strem Chemicals Inc., 99% stated purity). The external reservoir in which the $Co(CO)_3NO$ was held was heated to roughly 320 K for these experiments, and the pick-up conditions were such that acquisition of a single $Co(CO)_3NO$ molecule was more likely than pick-up of two $Co(CO)_3NO$ molecules. Experiments were also performed where C_{60} molecules were added to the helium droplets immediately after the addition of $Co(CO)_3NO$. The C_{60} (SES Research, 99.95% stated purity) was heated to a temperature of 558 K and added to the droplets in a second pick-up zone.

After picking up dopant molecules, the helium droplets passed through a skimmer to enter another differentially pumped vacuum chamber, where they were exposed to an electron beam of variable energy (0−150 eV). Any ions produced were then extracted into a high resolution and high repetition rate reflectron time-of-flight mass spectrometer (Tofwerk). This system can be used to explore both cations and anions, but in this particular study, we concentrate on anions generated by relatively low energy electrons. The electron energy was calibrated using the anion yield data collected by Engmann et al.[10,11] Anion yield curves derived from clusters and from $Co(CO)_3NO$ on C_{60} are hence referenced to gas phase measurements and are, therefore, corrected for the excess energy needed to inject electrons into liquid helium.[18,19] All anion yield curves have been corrected for background counts and isotopic effects of neighboring ions in the mass spectra.

RESULTS AND DISCUSSION

$Co(CO)_3NO$ Monomer. The presentation of our experimental findings begins with the observations for monomeric $Co(CO)_3NO$. Figure 1 shows ion yield curves as a function of electron kinetic energy for the eight anions detected. These range from the intact $[Co(CO)_3NO]^-$ parent anion through a series of fragment ions all the way down to Co^-. All of these anions were observed previously in gas phase work,[5,6] except for the parent anion. The observation of the latter in the current study is presumably the result of the very low temperature in a helium droplet, which, combined with the rapid dissipation of heat through evaporative loss of helium atoms,[20] should help to stabilize the anion. Nevertheless, $[Co(CO)_3NO]^-$ is not an abundant product when compared to the anionic fragments. Table 1 shows relative integrated peak areas between 0 and 20 eV to enable a comparison of ion abundances.

There are considerable similarities between the ion yield curves shown in Figure 1 and those reported by Engmann et al. in their gas phase studies,[10,11] particularly with regard to the energy of peak ion production and the widths of the observed resonances. However, there are also a couple of significant differences, and it is these differences which we focus upon here. First, we see a marked change in the shape of the ion yield profile for $[Co(CO)_2NO]^-$ when compared to the gas phase. Second, the most prominent anion seen in the helium nanodroplet experiments is not $[Co(CO)_2NO]^-$, as reported by Engmann et al., but is instead $[Co(CO)_2]^-$. In all other respects, the agreement with Engmann et al. is rather good.

The ion yield profile for $[Co(CO)_2NO]^-$ shows essentially three features. Two clear resonances with similar widths are seen at low energies, peaking at 1.6 and 4.3 eV. Although two peaks were seen by Engmann et al., these were at much lower energies (ca. 0 and 0.5 eV). Furthermore, in the gas phase, these two peaks had very different widths, with the higher energy peak being far more intense and much broader than the lower energy peak. Another major difference is that we see a broad and monotonically increasing ion yield above roughly 7 eV, whereas the gas phase work showed no production of $[Co(CO)_2NO]^-$ between 2 and 9 eV. At least, in part, we attribute this difference in behavior to quenching of reaction channels in helium droplets. In other words, resonances which would lead to certain fragments in the gas phase may be inhibited by rapid cooling in the helium nanodroplets, giving peaks in the yield of $[Co(CO)_2NO]^-$ at energies that would

DOI: 10.1021/acs.jpcc.5b05260
J. Phys. Chem. C 2015, 119, 20917−20922

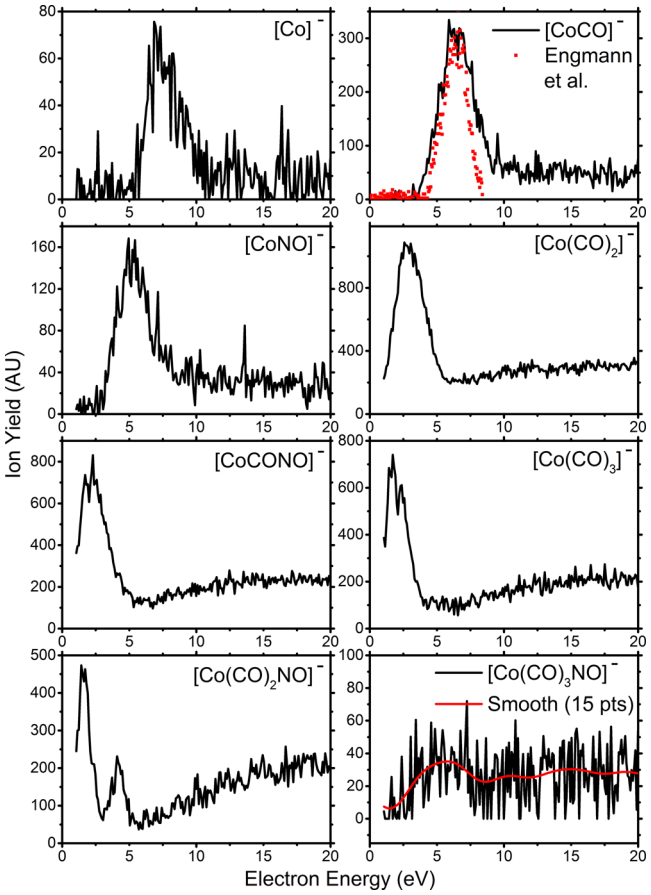

Figure 1. Yields for the parent anion, $[Co(CO_3NO]^-$, and its fragments as a function of electron energy. The signal/noise ratio for the parent anion in the bottom right panel is very low, and so the solid line (in red) through the data points was generated using data smoothing (15 pt FFT filter) to indicate how the yield varies with electron energy. To give some idea of the agreement between the helium droplet findings and the gas phase results obtained by Engmann et al.,[10,11] raw data for the $CoCO^-$ ion from the gas phase study have been incorporated into the upper right panel (shown by the data points marked in red). The agreement between the gas phase and helium droplet data for this ion is good, with only marginal broadening of the peak being seen in the helium droplet experiment. Similarly, good agreement is obtained for several other ions (not shown here), and any exceptions are discussed in detail in the main text.

Table 1. Relative Integrated Peaks Areas between 0 and 20 eV

ion	area
$[Co(CO)_3NO]^-$	0.07
$[Co(CO)_2NO]^-$	0.44
$[Co(CO)_3]^-$	0.56
$[Co(CO)NO]^-$	0.70
$[Co(CO)_2]^-$	1.00
$[Co(NO)]^-$	0.12
$[Co(CO)]^-$	0.22
Co^-	0.04

coincide with other reaction products if allowed to go to completion. Thus, the peak seen at 1.6 eV is close to the peaks seen for production of $[Co(CO)_3]^-$ and $[CoCONO]^-$, and thus quenching of these higher energy channels into the lower energy $[Co(CO)_2NO]^-$ channel might account for this peak. The peak at 4.3 eV overlaps with the low energy tail of the $[CoNO]^-$ resonance, perhaps indicating that this channel is quenched on the low electron energy side of this tail, leading to $[Co(CO)_2NO]^-$ production. The enhanced production of $[Co(CO)_2NO]^-$ above 7 eV may be the result of fragmentation of the dimer, $[Co(CO)_3NO]_2^-$, which shows much broader ion yield curves (see next section).

The most surprising observation for the monomer is that loss of a single CO molecule does not give the most prominent anion signal for helium nanodroplets, in marked contrast to the gas phase case. Since the DEA process with the lowest activation energy is expected to be loss of a single CO molecule, one might reasonably expect this route to be enhanced in helium droplets relative to the gas phase because of the quenching of secondary reactions. Instead, the combined loss of NO and a single CO molecule is found to be the most probable DEA process. We have calculated the energy required to eject various ligands from the parent anionic complex using the established quantum chemical extrapolation scheme CBS-QB3. In the CBS-QB3 model, geometries are optimized and the zero-point energy is evaluated by vibrational frequency calculations in the harmonic approximation using density functional theory (DFT) methodology. The obtained geometries are then used as a starting point for more accurate energy calculations, including extrapolation to the complete basis set limit.[21] The results are summarized in Table 2, which shows the energy required to break specific bonds in the parent anion at 0 K. The calculations conform to expectation, with the channel leading to loss of a single CO predicted to have by far the lowest threshold energy, 0.65 eV.

Table 2. Reaction Energies (0 K) Calculated Using the CBS-QB3 Model

reaction	ΔE/eV
$[Co(CO)_3NO]^- \rightarrow [Co(CO)_2NO]^- + CO$	0.65
$[Co(CO)_3NO]^- \rightarrow [Co(CO)_3]^- + NO$	1.56
$[Co(CO)_3NO]^- \rightarrow [Co(CO)NO]^- + 2CO$	2.36
$[Co(CO)_3NO]^- \rightarrow [Co(CO)_2]^- + CO + NO$	1.99

The preferential loss of CO rather than NO in the gas phase is presumably a consequence of statistical dissociation in the thermally activated initial state of the anion. However, the preferential ejection of CO + NO rather than a single CO molecule suggests that, in a helium droplet environment, the reaction process becomes constrained by specific dissociation dynamics. One possibility is that this process is assisted by a concerted rather than sequential loss of NO and CO from the parent anion. Concerted dissociation dynamics in DEA has been reported previously,[22] although we are not aware of any prior examples for metal-containing complexes.

$(Co(CO)_3NO)_N$ Clusters. Figure 2 summarizes the findings for the dimer of $Co(CO)_3NO$. Similar observations apply to the trimer, but the data in that case are of lesser quality than those for the dimer. The fragment ions detected are analogous to those identified from the monomer but are now attached to an intact $Co(CO)_3NO$ unit (which, for notational convenience, we will often refer to simply as M in the discussion below). The ion yield profiles for these clusters are dramatically different from those seen for the monomer. For the discussion that follows, we have assumed that peaks corresponding to the ions $[(M)_N(X)]^-$, where X is a fragment such as Co or $Co(CO)_2$, derive from the neutral species $(M)_{N+1}$. This assumption is

DOI: 10.1021/acs.jpcc.5b05260
J. Phys. Chem. C 2015, 119, 20917−20922

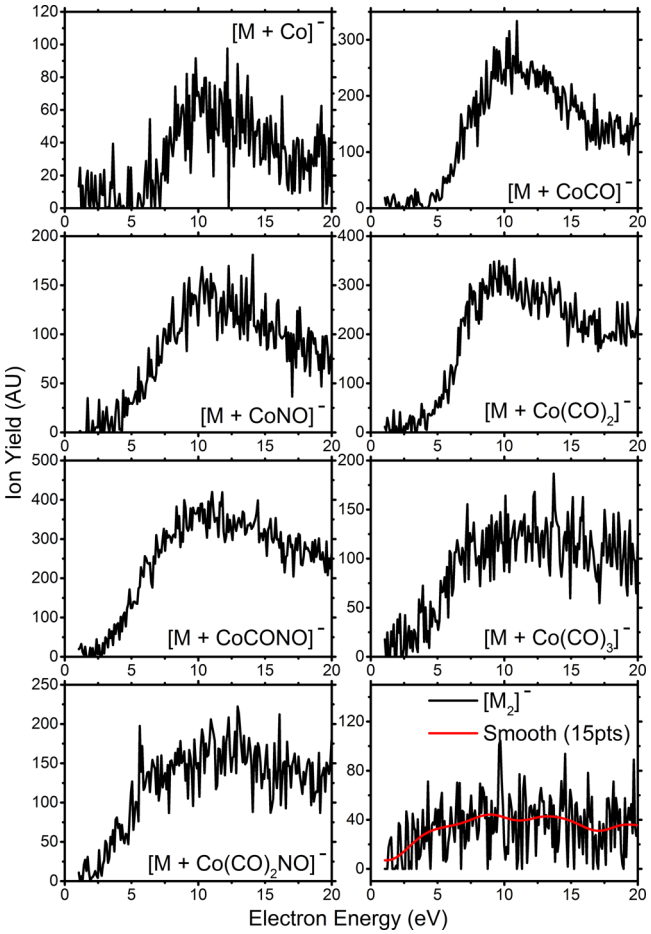

Figure 2. Yields for the parent dimer anion, $[Co(CO)_3NO]_2^-$ (here abbreviated as M_2^-), and smaller fragments of the type $[MX_nY_m]^-$ as a function of electron energy. A 15 pt FFT smoothing filter was used to generate the solid line (in red) in the bottom right panel.

necessary for a simple interpretation of the experimental data, but one should recognize that a cascade effect from larger clusters could contribute to the observed signals. This becomes particularly clear when looking at fragments of the form $[(M)_NCo_2(X)]$, which, for example, in the case of X = $(CO)_2NO$, are abundant and among the most remarkable peaks in the mass spectra (see Figure 3). These fragments necessarily stem from a neutral species of at least $(M)_{N+2}$. However, as Figure 3 clearly illustrates, fragments originating from $(M)_{N+3}$ also play a visible role. The yield curves in Figure 3 show a convergence in behavior with cluster size, suggesting that comparison with the condensed phase is already viable at these cluster sizes.

The most striking difference between the monomer ion yield plots in Figure 1 and the dimer plots in Figure 2 is that the latter are much broader and peak at far higher electron energies (in excess of 10 eV). Indeed, the anion yields arising from the monomer and dimer have almost nothing in common. Even the reaction probabilities are different, with the dimer no longer favoring loss of NO in preference to loss of a single CO. Instead, we see that the most abundant products correspond to loss of 2CO or CO + NO, with nearly equal probabilities at their peak electron energies. We still find, however, that loss of a single CO is not the most probable reaction outcome.

The source of the very different anion yield curves for the $Co(CO)_3NO$ monomer relative to its oligomers is not clear. It

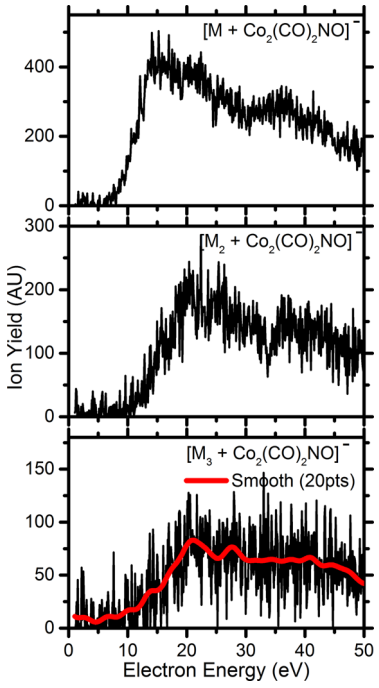

Figure 3. Yields for the anions $[M_nCo_2(CO)_2NO]^-$, where M = $Co(CO)_3NO$ and n = 1, 2, and 3. A 20 pt FFT smoothing filter was used to generate the solid line (in red) in the bottom right panel.

is possible that the oligomerization process has a profound impact on the electronic structure, perhaps because the monomer units interact rather strongly. In such cases, the electronic structure that must be considered is that of the supermolecule entity, rather than the monomers. An estimate of the dimerization energy of $Co(CO)_3NO$ would help to establish if this explanation is plausible, but this is beyond the scope of the current study. We must also consider the possibility that dissociative ion-pair formation (also known as dipolar dissociation) becomes an option for the oligomers. An example would be the CO-loss channel, the lowest energy dipolar dissociation channel, shown below:

$$[Co(CO)_3NO]_2 + e^- \rightarrow [Co(CO)_3NO]^+ + [Co(CO)_2NO]^- + CO + e^- \quad (2)$$

Since we do not know the dimerization energy of the neutral complex, we cannot calculate an accurate threshold energy for reaction 2. However, assuming a dimer binding energy of 1 eV and combining this with the known first ionization energy of $Co(CO)_3NO$ (8.33 eV[23]), the calculated electron affinity of $Co(CO)_3NO$ extracted in the current study (0.75 eV), and the energy required to remove a CO from the monomer anion shown in Table 2, we obtain an approximate energy threshold of 9.2 eV for reaction 2. This does not account for the tails to much lower electron energies seen in all of the anion yield curves shown in Figure 2, but it does suggest that dipolar dissociation channels could come into play at energies in the region of 10 eV.

The dramatic difference in DEA behavior between the $Co(CO)_3NO$ monomer and the dimer is important because it shows that the monomer is not a reliable guide to DEA behavior in an agglomerated sample such as a thin film, as would be the case in a real FEBID experiment. One important

DOI: 10.1021/acs.jpcc.5b05260
J. Phys. Chem. C 2015, 119, 20917−20922

consequence of the broad anion yield curves for $(Co(CO)_3NO)_N$ clusters is that a much wider range of electron kinetic energies can effect DEA than is implied by the quite strongly resonant behavior of the monomer. Accordingly, a much greater fraction of the available secondary electrons and backscattered electrons will be able to initiate decomposition if they are able to encounter a $Co(CO)_3NO$ film rather than the gaseous monomer.

$Co(CO)_3NO$ on C_{60}. Figure 4 shows the anion yield curves for products derived from $Co(CO)_3NO$ in combination with a

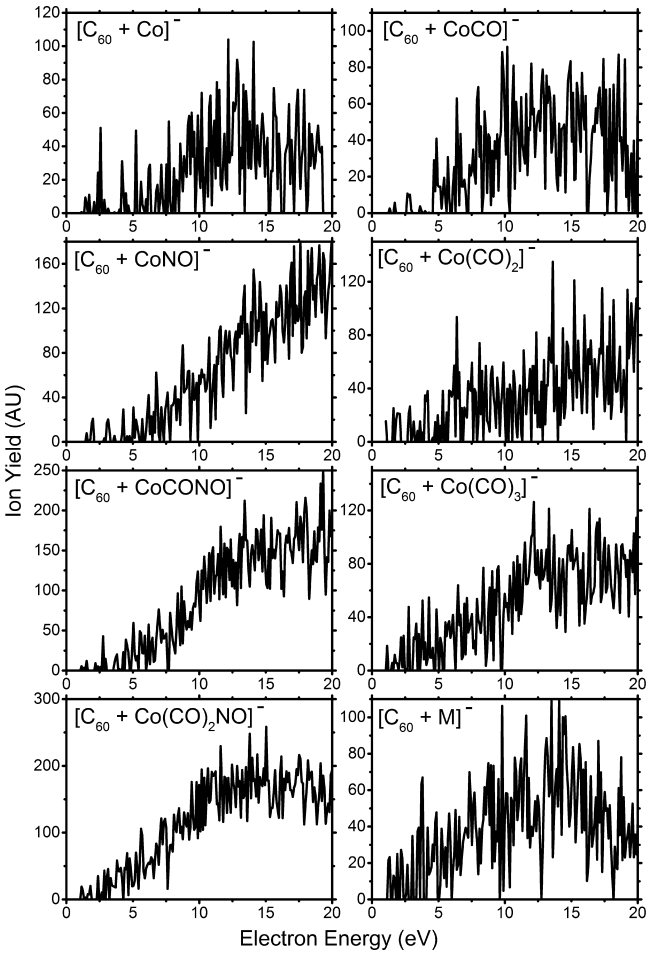

Figure 4. Anion yield as a function of electron energy for $Co(CO)_3NO$ combined with C_{60}.

single C_{60} molecule. The signal levels were not strong for these anions, and so the signal-to-noise ratios seen in Figure 4 are considerably worse than those in Figure 1. Nevertheless, some broad conclusions can be reached. First, the ion yield profiles have more in common with those seen for the $[Co(CO)_3NO]_2$ dimer than for the isolated monomer, in that the curves are very broad and peak at far higher electron kinetic energies than for the monomer. Since C_{60} has a reasonably high electron affinity (2.6835 ± 0.0006 eV[24]), which is comfortably in excess of that of $Co(CO)_3NO$ (0.75 eV according to CBS-QB3 calculations), low energy electrons might be expected to be preferentially injected into the C_{60} electronic manifold. However, while very broad anion yield curves have been recorded previously for C_{60} in helium, these peak near 5−6 eV.[25] The anion yield curves shown in Figure 4 are different, suggesting that, at the very least, there is funneling of excess energy into the $Co(CO)_3NO$ adsorbate, which can then initiate chemistry. However, another possibility is ion-pair formation leading to production of C_{60}^+ and the anion $[Co(CO)_3NO]^-$ and its fragments (dipolar dissociation), channels which will start to become energetically accessible at energies roughly exceeding 9 eV.

A notable difference in the anion chemistry between the $[Co(CO)_3NO]_2$ dimer and the behavior of monomeric $Co(CO)_3NO$ on C_{60} is that the loss of NO on electron attachment becomes a minor channel for $Co(CO)_3NO$ on C_{60}. We saw previously that, for $[Co(CO)_3NO]_2^-$, the losses of 2CO and NO + CO are the two most probable reaction outcomes, with almost equal cross sections. Furthermore, the loss of a single CO molecule is still a minor channel for the dimer. However, once C_{60} is present, the branching ratios change. The two most probable outcomes, with almost equal probabilities, are now for loss of either one or two CO molecules on electron attachment above 10 eV. Thus, when $Co(CO)_3NO$ is subjected to electron exposure when adsorbed on C_{60}, there is a far stronger propensity to retain NO than for either the isolated $Co(CO)_3NO$ monomer or its dimer.

We are not in a position to establish for certain why NO retention becomes more likely when $Co(CO)_3NO$ is located on C_{60}. However, one possibility is that the C_{60} surface might catalyze the dissociation of NO to form a Co−N bond. This suggestion is prompted by the observations by Rosenberg et al. on the electron-induced decomposition of $Co(CO)_3NO$ on a solid surface,[13] as discussed earlier. On the basis of X-ray photoelectron measurements, Rosenberg et al. proposed that decomposition occurs via formation of a Co−N bond and is summarized in reaction 1. One can imagine that, once such dissociation has occurred, the N and O atoms would be difficult to dislodge from the cobalt, in contrast to molecular NO. It would be interesting to explore whether or not this suggestion is applicable to $Co(CO)_3NO$ on C_{60}, perhaps by carrying out detailed *ab initio* calculations of the available reaction pathways and how these are affected by contact with a carbonaceous surface. Clearly, there are alternative explanations which might involve specific chemical binding of the parent anion or a fragment to C_{60}. A neat way to test this hypothesis would be to carry out similar experiments using a metallic cluster as the model surface to see if the substrate identity affects the DEA chemistry.

■ CONCLUSIONS

The effect of dissociative electron attachment to $Co(CO)_3NO$ in helium nanodroplets has been investigated for the first time. The anion yield curves for the monomer show similarities to those reported previously for gaseous $Co(CO)_3NO$. However, in helium nanodroplets, there are three notable differences: (1) observation of the parent anion, $[Co(CO)_3NO]^-$, albeit at very low abundance, (2) different resonances in the channel producing loss of a single CO molecule, and (3) a surprising preference for NO loss rather than CO loss. Observations (1) and (2) can be accounted for by quenching of certain reaction channels provided by the surrounding liquid helium. Observation (3) seems to be an effect delivered by constrained dynamics imposed by the liquid helium, although, at present, this is not fully understood. *Ab initio* calculations to establish the relevant potential energy surfaces and barriers to specific reaction channels would seem to be essential for resolving this matter.

DOI: 10.1021/acs.jpcc.5b05260
J. Phys. Chem. C 2015, 119, 20917−20922

For clusters of $Co(CO)_3NO$, the anion yield curves shift to higher electron energies and are much broader. The reaction probabilities also change, but the most dramatic effect is seen when $Co(CO)_3NO$ is located on the surface of C_{60}. Now, the loss of CO becomes the predominant reaction channel. It would be useful for an improved understanding of the FEBID mechanism to understand why the introduction of a surface induces this significant change in branching ratios. In particular, it will be important to establish if the surface catalyzes the decomposition of NO to form a cobalt oxynitride unit, as previously suggested by Rosenberg et al.[13]

AUTHOR INFORMATION

Corresponding Authors

*E-mail: Paul.Scheier@uibk.ac.at (P.S.).
*E-mail: andrew.ellis@le.ac.uk (A.M.E.).

Notes

The authors declare no competing financial interest.

ACKNOWLEDGMENTS

This work was given financial support by the Austrian Science Fund (FWF) Wien (P26635, P24443, and I978). We are also grateful for support for a short-term scientific mission funded by the EU Cost Action CELINA (CM1301). Oddur Ingólfsson is acknowledged for kindly providing raw data from previously published work, which was incorporated into Figure 1.

REFERENCES

(1) Utke, I.; Hoffmann, P.; Melngailis, J. Gas-assisted focused electron beam and ion beam processing and fabrication. *J. Vac. Sci. Technol., B* **2008**, *26*, 1197.

(2) van Dorp, W. F.; Hagen, C. W. A critical literature review of focused electron beam induced deposition. *J. Appl. Phys.* **2008**, *104*, 081301.

(3) Huth, M.; Porrati, F.; Schwalb, C.; Winhold, M.; Sachser, R.; Dukic, M.; Adams, J.; Fantner, G. Focused electron beam induced deposition: A perspective. *Beilstein J. Nanotechnol.* **2012**, *3*, 597−619.

(4) Gazzadi, G. C.; Mulders, H.; Trompenaars, P.; Ghirri, A.; Rota, A.; Affronte, M.; Frabboni, S. Characterization of a new cobalt precursor for focused beam deposition of magnetic nanostructures. *Microelectron. Eng.* **2011**, *88*, 1955−1958.

(5) Gazzadi, G. C.; Mulders, H.; Trompenaars, P.; Ghirri, A.; Affronte, M.; Grillo, V.; Frabboni, S. Focused electron beam deposition of nanowires from cobalt tricarbonyl nitrosyl ($Co(CO)_3NO$) precursor. *J. Phys. Chem. C* **2011**, *115*, 19606−19611.

(6) Vollnhals, F.; Drost, M.; Tu, F.; Carrasco, E.; Späth, A.; Fink, R. H.; Steinrück, H.-P.; Marbach, H. Electron-beam induced deposition and autocatalytic decomposition of $Co(CO)_3NO$. *Beilstein J. Nanotechnol.* **2014**, *5*, 1175−1185.

(7) Serrano-Ramón, L.; Córdoba, R.; Rodríguez, L. A.; Magén, C.; Snoeck, E.; Gatel, C.; Serrano, I.; Ibarra, M. R.; De Teresa, J. M. Ultrasmall functional ferromagnetic nanostructures grown by focused electron-beam-induced deposition. *ACS Nano* **2011**, *5*, 7781−7787.

(8) Boero, G.; Utke, I.; Bret, T.; Quack, N.; Todorova, M.; Mouaziz, S.; Kejik, P.; Brugger, J.; Popovic, R. S.; Hoffmann, P. Submicrometer Hall devices fabricated by focused electron-beam-induced deposition. *Appl. Phys. Lett.* **2005**, *86*, 042503.

(9) Utke, I.; Michler, J.; Gasser, P.; Santschi, C.; Laub, D.; Cantoni, M.; Buffat, P. A.; Jiao, C.; Hoffmann, P. Cross Section Investigations of compositions and sub-structures of tips obtained by focused electron beam induced deposition. *Adv. Eng. Mater.* **2005**, *7*, 323−331.

(10) Engmann, S.; Stano, M.; Matejčik, Š.; Ingólfsson, O. The role of dissociative electron attachment in focused electron beam induced processing: a case study on cobalt tricarbonyl nitrosyl. *Angew. Chem., Int. Ed.* **2011**, *50*, 9475−9477.

(11) Engmann, S.; Stano, M.; Papp, P.; Brunger, M. J.; Matejčik, Š.; Ingólfsson, O. Absolute cross sections for dissociative electron attachment and dissociative ionization of cobalt tricarbonyl nitrosyl in the energy range from 0 eV to 140 eV. *J. Chem. Phys.* **2013**, *138*, 044305.

(12) Papp, P.; Engmann, S.; Kučera, M.; Stano, M.; Matejčik, Š.; Ingólfsson, O. *Int. J. Mass Spectrom.* **2013**, *356*, 24.

(13) Rosenberg, S. G.; Barclay, M.; Fairbrother, D. H. Electron beam induced reactions of adsorbed cobalt tricarbonyl nitrosyl ($Co(CO)_3NO$) molecules. *J. Phys. Chem. C* **2013**, *117*, 16053−16064.

(14) Rosenberg, S. G.; Landheer, K.; Hagen, C. W.; Fairbrother, D. H. Substrate temperature and electron fluence effects on metallic films created by electron beam induced deposition. *J. Vac. Sci. Technol. B* **2012**, *30*, 051805.

(15) Warneke, J.; Van Dorp, W. F.; Rudolf, P.; Stano, M.; Papp, P.; Matejčik, Š; Borrmann, T.; Swiderek, P. Acetone and the precursor ligand acetylacetone: distinctly different electron beam induced decomposition. *Phys. Chem. Chem. Phys.* **2015**, *17*, 1204−1216.

(16) An der Lan, L.; Bartl, P.; Leidlmair, C.; Schöbel, H.; Jochum, R.; Denifl, S.; Märk, T. D.; Ellis, A. M.; Scheier, P. The submersion of sodium clusters in helium nanodroplets: Identification of the surface → interior transition. *J. Chem. Phys.* **2011**, *135*, 044309.

(17) Gomez, L. F.; Loginov, E.; Sliter, R.; Vilesov, A. Sizes of large He droplets. *J. Chem. Phys.* **2011**, *135*, 154201.

(18) Henne, U.; Toennies, J. P. Electron capture by large helium droplets. *J. Chem. Phys.* **1998**, *108*, 9327−9338.

(19) Denifl, S.; Zappa, F.; Mähr, I.; Lecointre, J.; Probst, M.; Märk, T. D.; Scheier, P. Mass spectrometric investigation of anions formed upon free electron attachment to nucleobase molecules and clusters embedded in superfluid helium droplets. *Phys. Rev. Lett.* **2006**, *97*, 043201.

(20) Toennies, J. P.; Vilesov, A. F. Superfluid Helium Droplets: A uniquely cold nanomatrix for molecules and molecular complexes. *Angew. Chem., Int. Ed.* **2004**, *43*, 2622−2648.

(21) Montgomery, J. A., Jr.; Frisch, M. J.; Ochterski, J. W.; Petersson, G. A. A complete basis set model chemistry. VI. Use of density functional geometries and frequencies. *J. Chem. Phys.* **1999**, *110*, 2822.

(22) Dąbkowska, I.; Flosadóttir, I. D.; Orzol, M.; Ptasinska, S.; Bald, I.; Ingólfsson, O.; Illenberger, E. Reactions in gas phase and condensed phase C_6F_5X (X = NCO, CH_2CN) triggered by low energy electrons. *Phys. Chem. Chem. Phys.* **2009**, *11*, 5323−5330.

(23) Sztáray, B.; Baer, T. Consecutive and parallel dissociation of energy-selected $Co(CO)_3NO^+$ ions. *J. Phys. Chem. A* **2002**, *106*, 8046.

(24) Huang, D.-L.; Dau, P. D.; Liu, H.-T.; Wang, L.-S. High-resolution photoelectron imaging of cold C_{60}^- anions and accurate determination of the electron affinity of C_{60}. *J. Chem. Phys.* **2014**, *140*, 224315.

(25) Jaksch, S.; Mähr, I.; Denifl, S.; Bacher, A.; Echt, O.; Märk, T. D.; Scheier, S. Electron attachment to doped helium droplets: C_{60}^-, $(C_{60})_2^-$, and $C_{60}D_2O^-$ anions. *Eur. Phys. J. D* **2009**, *52*, 91−94.

DOI: 10.1021/acs.jpcc.5b05260
J. Phys. Chem. C 2015, 119, 20917−20922